

HIFAN 1829

**Multi-channel optical pyrometer for
sub-nanosecond temperature measurements at
NDCX-I/II
by**

P.A. Ni, F.M. Bieniosek and W.L. Waldron

from
Lawrence Berkeley National Laboratory (on behalf of U.S. HIFV-VNL)
1 Cyclotron Road, Berkeley, CA 94720
Accelerator Fusion Research Division
University of California
Berkeley, California 94720

April 2011

This work was supported by the Director, Office of Science, Office of Fusion Energy Sciences, of the U.S. Department of Energy under Contract No. DE-AC02-05CH11231.

This document was prepared as an account of work sponsored by the United States Government. While this document is believed to contain correct information, neither the United States Government nor any agency thereof, nor The Regents of the University of California, nor any of their employees, makes any warranty, express or implied, or assumes any legal responsibility for the accuracy, completeness, or usefulness of any information, apparatus, product, or process disclosed, or represents that its use would not infringe privately owned rights. Reference herein to any specific commercial product, process, or service by its trade name, trademark, manufacturer, or otherwise, does not necessarily constitute or imply its endorsement, recommendation, or favoring by the United States Government or any agency thereof, or The Regents of the University of California. The views and opinions of authors expressed herein do not necessarily state or reflect those of the United States Government or any agency thereof or The Regents of the University of California.

Multi-channel optical pyrometer for sub-nanosecond temperature measurements at NDCX-I/II.

P.A. Ni, F.M. Bieniosek and W.L. Waldron

We present a detailed technical description of a fast multi-channel pyrometer designed for warm-dense-matter (WDM) experiments with intense heavy ion beams at the neutralized-drift-compression-experiment linear accelerator (NDCX-I/II) at Lawrence Berkeley National Laboratory (LBNL). The unique features of the described instrument are its sub-nanosecond temporal resolution (100 ps rise -time) and a broad range, 1,500 K – 12,000 K of measurable brightness temperatures in the visible and near-infrared regions of the spectrum. The working scheme, calibration procedure, experimental data obtained with the pyrometer and future applications are presented.

Introduction

Warm-dense-matter (WDM) is characterized by near solid-state densities, temperatures up to 100,000 K and several Mbar pressure. These states are relevant to the fields of plasma physics, astrophysics, geophysics, planetary science, etc [Davidson]. An extensive WDM research campaign with intense heavy ion beams was launched at LBNL in 2008 [Bieniosek, Seidl]. The ultimate goal of the experiments is to investigate properties of matter under extreme conditions, in particular, to study the equation of states (EOS) of metals near melting, in the two phase liquid-vapor and critical regions of the phase diagram [Davidson, Barnard]. In general, temperature, pressure and density must be known for a complete thermodynamic description of matter. This paper focuses on temperature diagnostics on NDCX-1, in particular, on a recently fielded multi-channel pyrometer.

The existing NDCX-I delivers sufficient beam intensity to allow for generation of low-temperature, two phase liquid-vapor states. It is expected that the next generation NDCX-II machine [Friedman] under construction at LBNL (to be commissioned in 2012) will have enough beam energy to reach temperatures up to 30,000 K, enabling the study of properties of matter near its critical point, the least studied part of the phase diagram.

The present NDCX-I accelerator (K^{+1} , 300 keV) heats targets up to 4,000 K and depending on the objective of an experiment, ion beam bunch duration can be varied from 2 ns to tens of microseconds. The pyrometer presented in the paper has been designed primarily for experiments with 2 ns heating pulses, where sub-nanosecond temporal resolution is required. During the course of an experiment, a sample passes through melting, evaporation and solidification phases. Therefore, it is required that a temperature diagnostic has enough dynamic range to measure temperature of all phase transitions in a single record.

In general, sub-nanosecond temporal resolution for an optical instrument is not an exceptionally requirement, especially if one considers laser experiments with sub-picosecond heating pulses. However, in contrast to the laser experiments, where samples are heated easily to 10,000 -100,000,000 K (several MW/cm²/nm/sr of thermal photons) temperatures obtained with the heavy-ion beams do not exceed 4,000 K, (typical emission level is several μW/cm²/nm/s) and hence number of photons available for diagnostic is much lower. The effective amount of light available for diagnosis is also limited, because thermal light must be probed from a sub-millimeter area, within the millimeter-size NDCX-1 focal spot.

Detection of micro-watt radiation emitted at sub- nanosecond time scale approaches the sensitivity threshold of present high-speed detectors. This constitutes the main technical challenge of the presented work. Many high-speed pyrometers with sufficient sensitivity have been built [see Ni and references therein], but we are not aware of any documented pyrometer with sub-nanosecond temporal resolution. The typical rise-time of published pyrometers varies from a millisecond to several nanoseconds.

Construction

In essence, a pyrometer is an absolutely calibrated spectrometer operating at several discrete wavelengths in the (vis) and near-infrared (nir) regions of the spectrum. The operating principle is based on the comparison of thermal radiation at a given wavelength to black-body radiation related to the temperature via the Planck formula [Michalski].

In the design of the instrument, speed determining factors, i.e. modal dispersion of fibers, rise-time of photodiodes, bandwidth of oscilloscope, must be taken into account. It should also be kept in mind that with an increase in temporal resolution, the sensitivity of a detector decreases, thus requiring a compromise between speed and sensitivity.

Light collection system (LC). Thermal emission from an ion-beam-heated metal target is collected by a relay system of lenses (a pair of achromatic doublets, f=75, d=50.8 mm coated for vis-nir) mounted on a motorized micro-positioning stage in vacuum. The lens system produces a 1:1 imaging of the target on an optical fiber, which transfers the light from the vacuum chamber to a pyrometer or a spectrometer. The optics is oriented normally to the sample surface (figure 1).

Probing spot-size is determined by the diameter of the fiber core. For efficient coupling of collected light into the optical fiber, the focus and aperture of the lenses were chosen to match the NA=0.2 numerical aperture, which corresponds to a 24° acceptance angle. Step-index, multimode, 200 μm or 400 μm diameter, silica fiber was used in the experiments. A smaller probing spot is favorable due to a higher degree of temperature homogeneity within the probing area, but at the same time, it reduces the sensitivity of the instrument. The NDCX-I focal spot has a Gaussian-like transverse intensity distribution with ~ 1 mm FWHM. A 400 μm diameter fiber is a satisfactory compromise between the level of signal, spatial resolution, and homogeneity.

On a sub-nanosecond time scale, modal dispersion (a distortion mechanism occurring in multimode fibers, in which the signal is spread in time because the propagation velocity of the optical signal is not the same for all modes) must be taken into account. One meter of a step-index 400 μm fiber introduces ~ 50 ps modal dispersion [Palais]. The length of fiber in the pyrometer was 2 m, which restricted the temporal resolution to ~ 100 ps. There are two ways to further reduce modal dispersion: to use a single mode fiber or use a graded-index, multimode fiber. In comparison to multimode step-index fibers, these types have a lower light-coupling efficiency, since they normally have a smaller diameter and smaller NA.

Note that if sufficient signal is available (e.g. higher temperatures), the probing size can be reduced to 50 μm (smallest commercially available diameter) and the graded-index fiber solution can be used for faster rise-times.

Spectral resolution. The spectral resolution scheme employed in the pyrometer is explained in figure 1. The same ray of light passes through a set of spectrally-selective beam splitters (later also referred to as channels and mirrors), A, B, C, E, F, G. The first beam splitter, A, separates vis (≤ 900 nm) light from NIR light, while beam splitters B, C, E, F, G act as mirrors for a narrowly specified spectral bandwidth and are transparent for the rest of the spectrum. After passing through the entire array of mirrors, the remaining portion is detected by channels G and D. The light spectrum at a channel is a product of the transmission/reflection of the beam splitters preceding a given channel.

The beam splitters are a custom product manufactured by the Tower Optics Corporation. They consist of a computer-optimized dielectric coating on a 1 mm thick, 25 mm diameter glass substrate. Mirrors A, B and C are designed to work at 30° of incidence, while E, F, G are designed to work at 45° . All of the mirrors are designed to have no polarization dependence of reflectivity under the specified angles of incidence. In order to maintain this condition, light from the coupling fiber is initially collimated by an achromatic doublet ($f=25$ mm) and re-focused at a photo detector by a coated aspherical lens ($f=12$ mm) after passing through the sequence of mirrors.

In figure 2, the effective transmission, $F_i(\lambda)$ at each channel is plotted, which is derived from a sequential multiplication of real transmission curves provided by the manufacturer. The channels are centered at 600 nm, 750 nm, 900 nm, 1050 nm, 1200 nm, 1350 nm and 1500 nm, with 150 nm effective widths. The wavelength range was chosen to cover the Planck curve peak corresponding to the 1,000 -10,000 K temperature range.

In the present configuration the entire 150 nm bandwidth is used. If narrower spectral width should be required, there is a reserved slot in front of each detector to accommodate an additional one inch interference filter. Adding a narrower band-pass filter for present low-level radiation (temperature) levels, will significantly reduce the sensitivity of the instrument.

Separation of vis and NIR by splitter A significantly simplifies the design of the coatings and allows for the exclusion of secondary filters for suppression of higher-order

reflections. The absence of the suppression filter, combined with a coating optimized for best possible efficiency, result in an overall transmission close to 90%. These custom filters are one of the key components responsible for the high performance of the instrument. For a comparison, the maximum transmission of a band-gap interference filter varies from 20% to 60%.

Light detection. Finding a suitable detector was a major challenge during the construction of the instrument. A critical requirement is a broad frequency response current amplifier with a flat gain curve between the required low and high cut-off frequencies. For this application, the high cut-off frequency should be several GHz and the low cut-off is DC. The DC response is essential for calibration, since pyrometers are calibrated with continuous radiation sources. Further requirements include sensitivity in the vis and nir regions of spectrum, linear response, low noise level, broad dynamic range, and low price since multiple channels are required.

After considering various options including avalanche photo diodes, photomultiplier tubes (PMT), micro-channels plates (MCP) and PIN photodiodes from several manufacturers, amplified PIN photo diode models 1591 and 1592 from Newfocus Inc were selected. The other photo-receivers, which were considered have a low-frequency cut-off starting from 10 kHz, making the calibration of a pyrometer difficult. Avalanche photodiodes and PMTs exhibit high noise levels and saturate quickly, which limits the dynamic range of the instrument. PMTs and MCPs contain a phosphor which chemically degrades with time, requiring frequent re-calibrations. PMTs and MCPs also have a high average cost per unit.

The critical feature of the chosen detectors is a flat gain curve from DC to 4.5 GHz (model 1590) and DC to 3.5 GHz (model 1591), resulting in 50 ps and 75 ps rise times respectively. Spectral response of the 1591 GaAs detectors matches the spectral requirements of channels B, C, D, while the 1592 InGaAs detectors are best suited for channels E, F, G and H. All of the electrical connections are made with coaxial cables (SMA), and 50 Ohm terminations. The data is acquired by a Tektronix 2.5 GHz, 40 GS/s oscilloscopes.

Due to the high combined price of a detector unit and a GHz-capable digitizer channel, the present design has only three detectors installed at channels C, E and G. All of the beam-splitters depicted in figure 1 had to be installed in order to maintain the designed spectral bandwidth at the channels with detectors. The system can be easily upgraded up to maximum of 7 channels.

The average 500 V/W sensitivity of the Newfocus photo-receivers is relatively low in comparison to the sensitivity of the other detector options (5-10 kV/W). Therefore in order to compensate for this low gain, efficient light coupling and spectral resolution described above was critical.

Calibration and data processing. The pyrometer is calibrated against a NIST traceable tungsten ribbon lamp at a physical temperature of 2,600 K. Specific details of the calibration procedure are straight forward and can be found in [Ni].

During calibration, all optical components (collection lenses, vacuum feed-throughs, fiber, etc.) are the same as in the actual target experiments. Real beam splitter transmission/reflection curves are used for calculation of calibration coefficients and temperature processing. Table 1 summarizes the calibration coefficients as well as the lower and upper bounds of the black-body temperature detection limits.

Table 1:

Channel	Calibration [W/V]	min T, [K]	max T, [K]
C (750 nm)	~1,900	~1,900	~12,000
E (1000 nm)	~700	~1,700	~13,000
G (1350 nm)	~800	~1,500	~30,000

The minimum temperature corresponds to the 5 mV rms detector noise level, and the maximum temperature is determined by the 1 V saturation voltage of an amplifier under CW radiation. Note that channel G has a much broader temperature range, which is explained by the exponent structure of the Planck formula; when temperature increases, a peak of the Planck curve shifts to shorter wavelengths, resulting in the uneven growth of radiation with temperature at different wavelengths.

Experimental data processing is straightforward: due to the linear response of the detectors, absolute light intensity $I_i(\lambda)$ is merely a product of calibration coefficients and voltage output of a detector. Absolute intensities, $I_i(\lambda)$ at each channel is related to brightness temperature, T_i through the expression

$$I_i(\lambda) = \int F_i(\lambda) \cdot \frac{C_1}{\lambda^5} \frac{1}{e^{\frac{c_2}{\lambda \cdot T_i}} - 1} \cdot d\lambda$$

Because the filters are relatively wide, the integral equation is solved numerically in MATLAB, instead of applying a narrow filter approximation (which would normally exclude the integral [Ni]).

Experimental results

Figure 3 shows brightness temperatures recorded by the pyrometer in an experiment where a 150 nm thick gold foil was heated by the NDCX-I ion beam. The foil was pre-heated by a microsecond pre-pulse and then rapidly heated by a 2 ns bunch-compressed portion of the beam arriving at 1600 μ s relative to the head of the pulse.

For a reference, a simple numerical simulation of the expected evolution of temperature in the experiments is shown as well. The simulation model assumes a realistic energy beam flux and table data of heat capacity and heat conduction of gold. The model includes radiation, Richardson and evaporation cooling mechanisms but does not take

into account any hydrodynamic instability, i.e. Rayleigh-Taylor and droplet formation mechanism.

A large discrepancy from the simulation can be explained by the incomplete model, as well as the fact that the simulation produces physical temperature while the pyrometer measures black body temperature. In order to match a simulation to an experiment, one must know the spectral emissivity [Michalski]. In most of WDM dynamic heating experiments, the emissivity is not known and must be measured independently, e.g., with laser ellipsometry [Yoneda].

To test the instrument at its upper bandwidth limits, an additional series of experiments were carried out, where 150 nm copper foils were heated by a 200 mJ, 100 fs laser pulse (figure 4). In these tests we used only the E (1050 nm) channel. The “ringing” structure seen in the records is a distortion induced by the limited bandwidth of the detectors. The manifestation of the distortion is consistent with the claimed 4.5 GHz bandwidth, when the response time of the instrument is much longer than the laser pulse duration.

Summary

We describe a fast multi-channel pyrometer and analysis of experimental results. We point out the technical difficulties associated with sub-nanosecond response time as well as other limitations of the instrument, such as sensitivity and speed.

NDCX-II is currently being built and is scheduled for commissioning in late 2012. This new accelerator will significantly expand the WDM research program at LBNL as it will give access to higher temperature regions. It is estimated that NDCX-II will be capable of heating solid matter up to 30,000 K in less than a nanosecond, thereby making the presented instrument more relevant to the future experiment. Due to the higher temperature, more thermal light will be available for analysis, and as it has been described, temporal, spectral and spatial resolution of the instruments can be improved without major hardware modifications.

Acknowledgments

This work was performed under auspices of the U.S. Department of Energy under Contracts No. DE-AC02-05CH11231 and DE-AC52-07NA27344. The authors would like to thank Dr. Dmitry Nikolaev from IPCP, Russia for critical comments and consultations and Dr. Chris Weber for testing the pyrometer in the laser experiment.

References

[Barnard] J. J. Barnard, J. Armijo, R. M. More, A. Friedman, I. Kaganovich, B. G. Logan, M. M. Marinak, G. E. Penn, A. B. Sefkow, P. Santhanam, P. Stoltz, S. Veitzer, J.S. Wurtele, "Theory and Simulation of Warm Dense Matter Targets," Nuclear Instruments and Methods in Physics Research A, 577, (2007), 275-283.

[Bieniosek] F.M. Bieniosek, J.J. Barnard, J.E. Coleman, E. Henestroza, M.A. Leitner, B.G. Logan, R.M. More, P.A. Ni, P.K. Roy, W.L. Waldron, P.A. Seidl, “HIGH ENERGY

DENSITYPHYSICS EXPERIMENTS WITH INTENSE HEAVY ION BEAMS”, Heavy Ion Fusion Symposium 2008, Tokyo, Japan, August 2-9, 2008, LBNL-942E.

[Davidson] FRONTIERS IN High Energy Density Physics: THE X-GAMES OF CONTEMPORARY SCIENCE, NATIONAL RESEARCH COUNCIL OF THE NATIONAL ACADEMIES

[Friedman]DEVELOPING THE PHYSICS DESIGN FOR NDCX-II, A UNIQUE PULSE-COMPRESSING ION ACCELERATOR

[Michalski] L. Michalski, K. Eckersdorf, J. Kucharski, J.McGhee, Temperature Measurement Second Edition, 2001 John Wiley

[Ni]P.A. Ni, M.I. Kulish, V. Mintsev, D.N. Nikolaev, V.Ya. Ternovoi, D.H.H. Hoffmann, S. Udrea, A. Hug, N.A. Tahir, D. Varentsov, “Fast six-channel pyrometer for warm-dense-matter experiments with intense heavy-ion beams”, Laser and Particle Beams, December 2008, LBNL-1260E.

[Palais] Palais, C. J., *Fiber Optic Communications*, Prentice-Hall, Inc., Englewood Cliffs, NJ, 1984

[Seidl] P.A. Seidl, A. Anders, F.M. Bieniosek, J.J. Barnard, J. Calanog, A.X. Chen, R.H. Cohen, J.E. Coleman, M. Dorf, E.P. Gilson, D.P. Grote, J.Y. Jung, M. Leitner, S.M. Lidia, B.G. Logan, P. Ni, P.K. Roy, K. Van den Bogert, A.B. Sefkow, W.L. Waldron, D.R. Welch, “PROGRESS IN BEAM FOCUSING AND COMPRESSION FOR WARM-DENSE MATTER EXPERIMENTS”, Heavy Ion Fusion Symposium 2008, Tokyo, Japan, August 2-9, 2008, LBNL-1072E.

[Yoneda] H. Yoneda, H. Morikami, K. Ueda, R. M. More, Phys. Rev. Lett. 91, 075004 (2003).

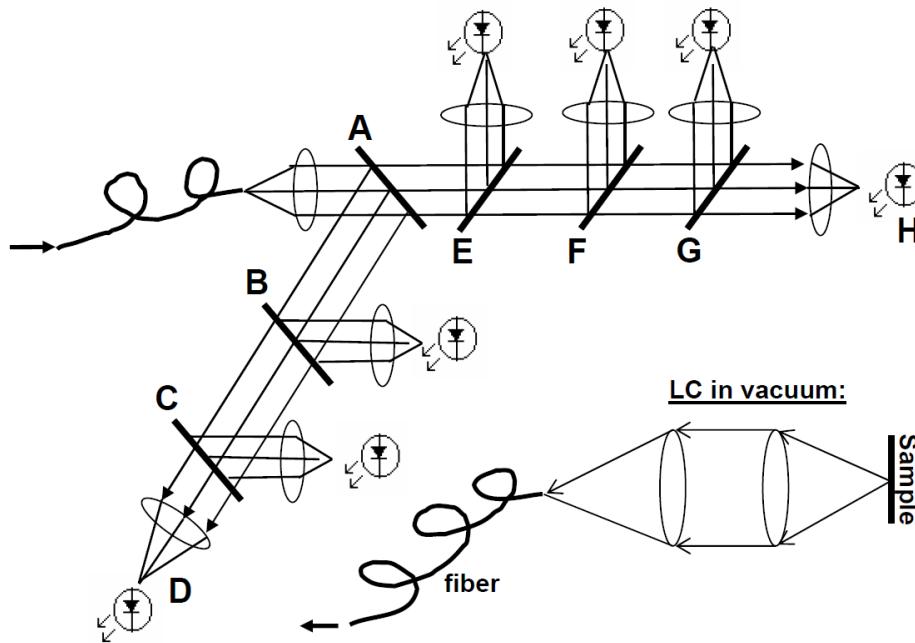


Figure 1: Light collection (LC) and spectral resolution scheme of pyrometer (shown seven-channel version).

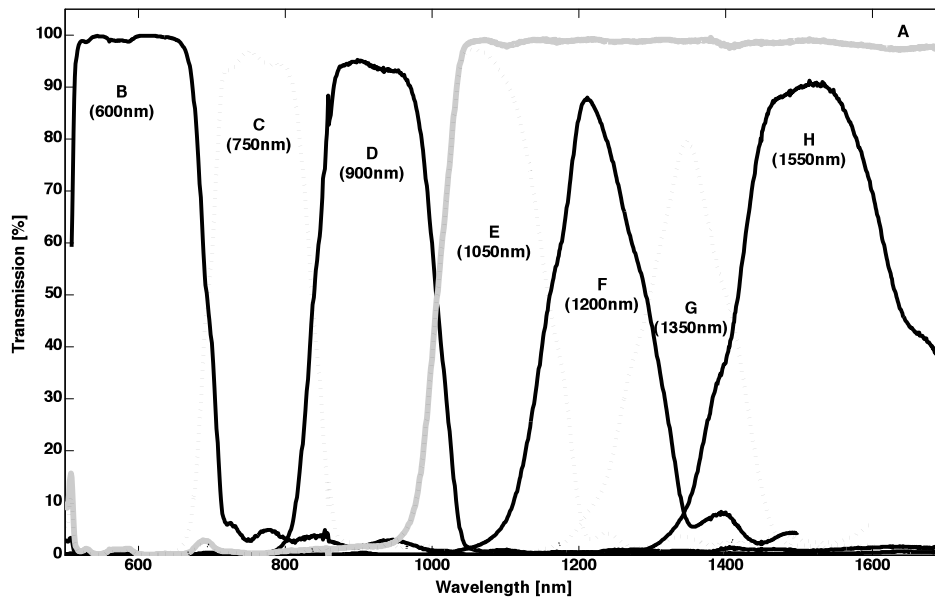


Figure 2: Effective spectral bandwidth of pyrometer channels (center wavelength shown in brackets) and spectral characteristic of beam splitter A (gray). Curves are calculated using real transmission data.

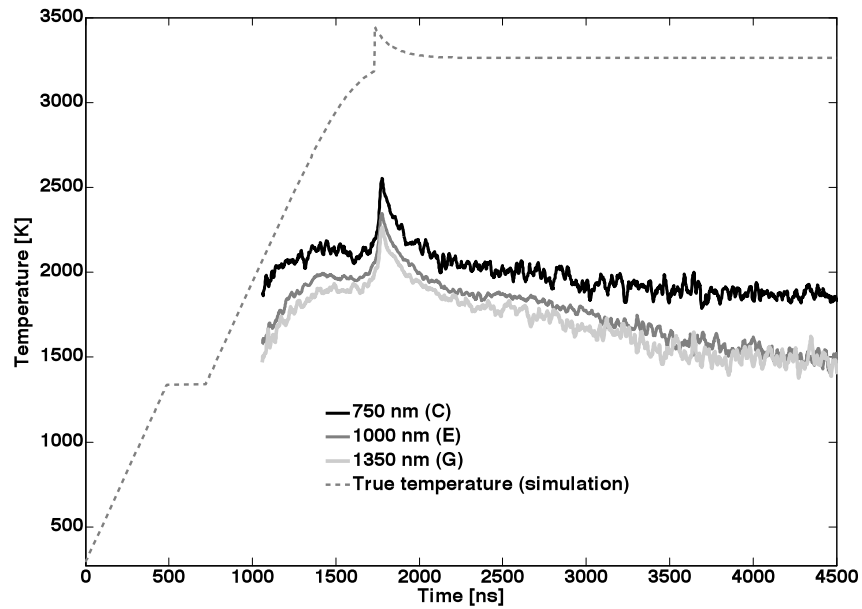


Figure 3: Brightness temperatures of an ion-beam heated gold target and the corresponding simulation (dashed). The uncompressed part of the beam hits the target at 0 ns, followed by a 2 ns compressed bunch at 1,600 ns.

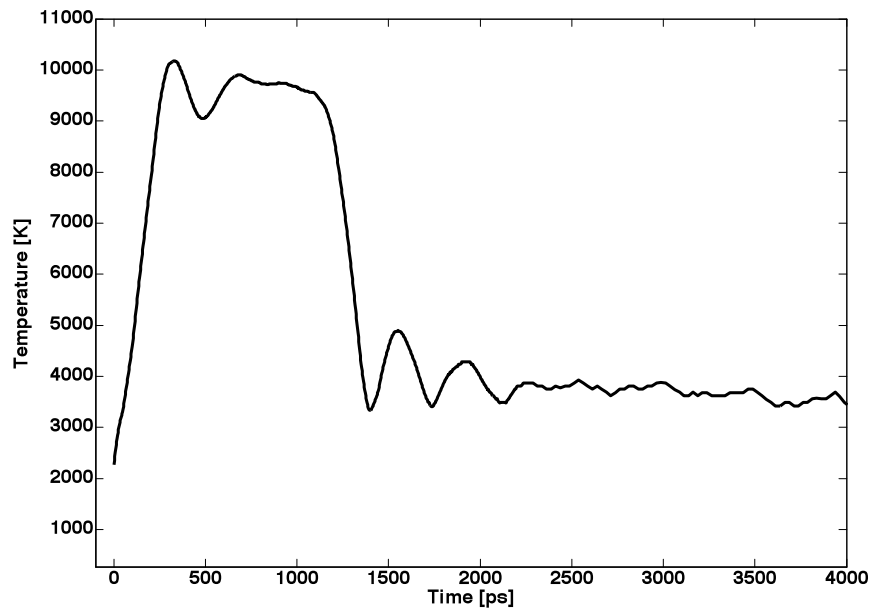


Figure 4: The brightness temperature at 1000 nm of a laser-beam heated copper target. The 100 fs laser pulse arrives at 0 ps. The “ringing” of the signal is instrumental and caused by the limited frequency bandwidth of the instrument.